

# Chapter 12

## Integration of Terrestrial Laser Scanning and GIS Analysis for Multi-temporal Landslide Monitoring: A Case Study of the Mont de La Saxe (Aosta Valley, NW Italy)



Gianpiero Amanzio, Ashwani Kumar Tiwari, Muriel Lavy,  
and Marina De Maio

**Abstract** In Italy, landslide phenomena and mass movements are very common, particularly along the Alps, the principal mountainous chains in the northern part of the country. In this study, we used a terrestrial laser scanner (TLS) to collect a multi-temporal dataset during 3 years (2012–2014) of observation, with the aim of accurately evaluating these phenomena in the Mont de la Saxe area (Aosta Valley region, Italy). Starting from the point clouds acquired with the TLS, we derived the digital surface models and we performed a multitemporal analysis in geographical information system (GIS) to identify the morphological features of the landslide and to delineate the displacement of the phenomena. The analysis allows quantifying the major elevation change occurred in the middle and the bottom side of landslide body during 2012–2014 with a high precision. The volume displaced in the second year (2013–2014) increased by 66% than the previous year (2012–2013), showing a progressive acceleration of the landslide phenomena. This result indicates that the volume estimation is crucial for planning future landslide emergency situations and to calibrate the early warning system, based on occurred phenomena.

**Keywords** Terrestrial laser scanning (TLS) · Landslide · Mont de La Saxe · Mass movement, DTM · GIS

---

G. Amanzio (✉) · M. Lavy  
GENEGIS GI S.r.l., Turin Branch (TO), Turin, TO, Italy  
e-mail: [g.amanzio@genegis.net](mailto:g.amanzio@genegis.net)

A. K. Tiwari · M. De Maio  
DIATI-Department of Environment, Land and Infrastructure Engineering  
Politecnico di Torino, Torino, Italy

## 12.1 Introduction

A landslide is when rock, debris or earth move down a slope. Landslides occur when the materials which constitute the slope of a hill fail and the force of gravity intervenes. The failure of materials that produces a landslide can be the result of natural causes or human activity. Specifically, natural activities like heavy or long-lasting rainfall, melting snow, and rapid tectonic forcings, for example, volcanic activity or earthquakes, are trigger factors for landslides. Moreover, landslides occur due to human activities such as changes in the slope profile, excavation, irrigation deforestation and other factors [1]. Landslides are the cause of several adverse effects on many environmental elements such as a change in the topography surface; contamination of the quality of rivers and streams as well as the groundwater flow system; forest cover loss, and impact on the habitats of natural wildlife living on the earth's surface [2]. In recent time, several studies from different countries have used different methods to evaluate the landslides problems [3–11]. Landslide phenomena frequently occur in Italy, notably in the principal mountain chains like the Apennines or the Alps [12].

In fact, because of characteristic like its relief, lithology, and structure in Italy the risk of the landslide is very high. They occur throughout Italy and are the most frequent type of natural disaster. After earthquakes, landslides are responsible for the highest number of victims [13]. In the last 30 years, there have been disastrous landslides in Piemonte (1994), Sarno and Quindici (1998) and NW Italy (2000). Specifically, the Aosta Valley (NW Italy), where is located the case study discussed in the following, is a prevailing mountain territory particularly prone to arising from landslides phenomena. Among them, we can mention Becca France landslide [14], Beaugard landslide [15] and Bosmatto landslide [16].

In order to manage the risk deriving from landslide phenomena, geographical information system (GIS) spatial analysis is one of the most prominent effective techniques in order to map zones and assess risk regarding environmental health problems [17–19]. The handling and analyzing through spatial data tools of GIS software could make the application of quantitative analysis in landslide hazard assessment and mapping easier [20]. Some of these techniques monitor landslides using laser scanner instrumentation based on Light Detection and Ranging (LiDAR) technology. Geographical information system (GIS) represents a useful tool when quick decisions are required because graphical representation facilitates a policy decision making [21]. Several researchers have used GIS technique for the evaluation of the hazardous risk of landslides on the environmental parameters as well as mapping of landslides [22–31].

Furthermore, the use of Terrestrial Laser Scanner (TLS) represents an advanced approach to monitor instability phenomena and to detect the landslide displacement [32]. The intense use laser scanning technology, with automatic filter procedures allows a rapid high resolute Digital Terrain Models (DTM) production, with high accuracy and high automation which is crucial for a multitemporal monitoring system [33]. The landslide area is often characterized by a hard accessibility due

to the high level of risk of moving around the dangerous area, for this reason, the use of long-range laser scanner represents a safety technique of monitoring without decrease the accuracy and the resolution during the survey [34]. Thus, the aim of this study was to identify the landslide phenomenon using TLS and GIS techniques in the Mont de La Saxe, Aosta Valley region. The information on the landslide phenomenon is very useful for the management of landslides in the area. It could also assist policy makers to tackle landslides in the area.

## 12.2 Study Area

The case study of the Mont de La Saxe landslide is situated in the Aosta Valley (NW Italy) in the Courmayeur municipality above the La Saxe hamlet (Fig. 12.1). In Italy, there are a lot of complex landslides and the one present on the Mont de La Saxe is one of these. The volume estimation raises about 8 million cubic meters [35], generating great risks for the small communities of La Palud and Entrèves. National and international viability is also affected, as this spot is crucial due to the nearby International Mont Blanc Tunnel. In the spring of 2013 a sudden acceleration occurred in the landslide body, so the local administration had to evacuate the area, closing any access to the Ferret Valley [36]. Mapping extant slope failures are thought to be the principal tool for assessing landslide phenomenon [37]. In landslide studies, high-resolution Digital Terrain Models (DTMs) allows analysis of the morphological features of the landslide slope, which are necessary to understand the space-and time-dependent processes. LiDAR (light detection and ranging)-derived DTMs are extensively used to study the landslide, focusing on estimating the volume, boundary and topographic change of landslides [38–40]. So, data collected by long-range terrestrial laser scanner are processed in a GIS with the aim to extract the landslide morphological features of rapid movement and to generate high resolute DTM.

### 12.2.1 *Climate and Geological*

The Aosta Valley is a mountainous region in northwestern Italy and it is intersected by glacial tributaries, creating eighteen minor valleys, mainly along the North-South axis and converging towards the Aosta Valley. The Dora Baltea River is the principal water course, flowing West to East.

A typical alpine climate dominates in the Aosta Valley region with very low temperature in winters and cool summers. The Aosta Valley has a significant amount of rainfall during the year. Specifically, it is highest peaks in autumn and spring, and lowest in winter and summer. In fact, the peak mean precipitation is approximately 140 mm of rainfall in a month, and the minimum value is 30 mm [41].

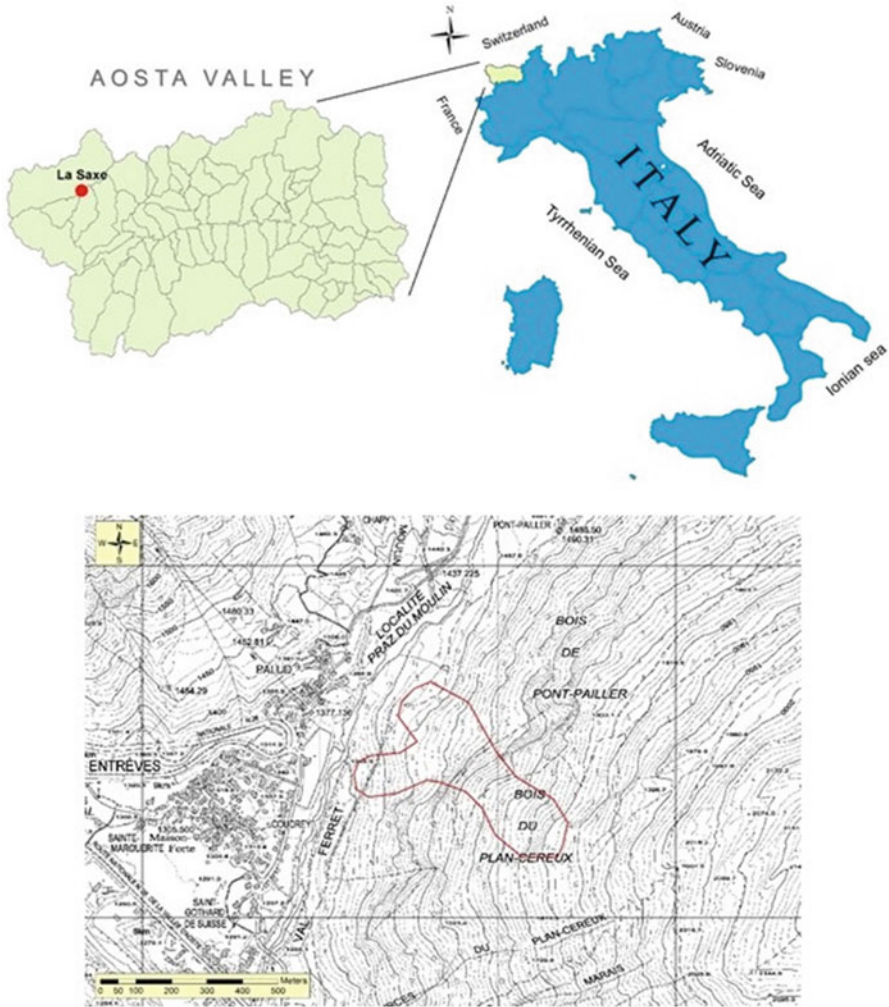
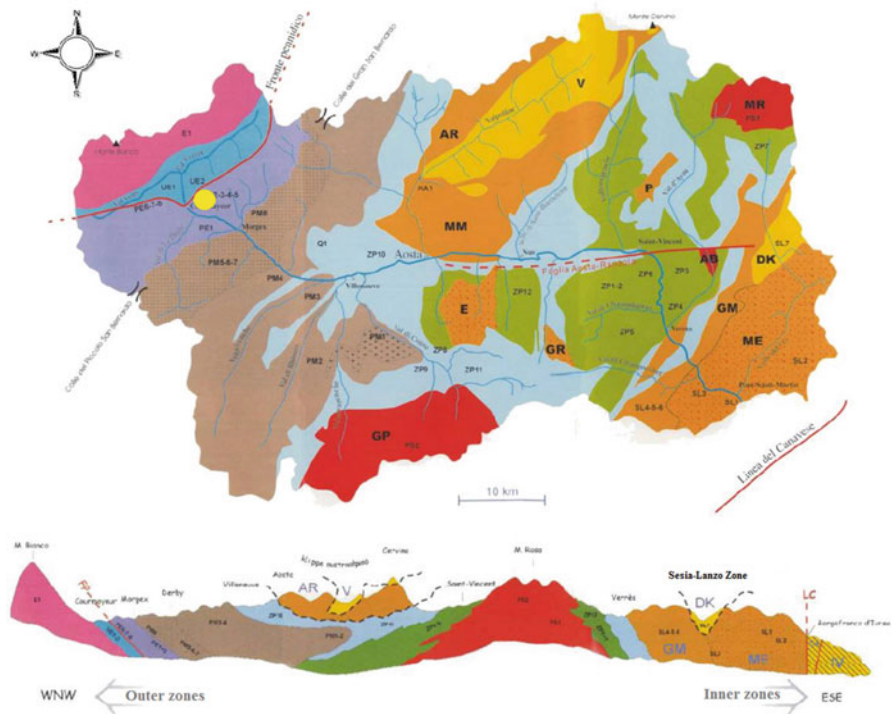


**Fig. 12.1** Test sites location (red polygon) at the Mont de La Saxe of the Aosta Valley region, Italy

The alpine range comprises a number of crystalline and metamorphic tectonic domains. It is from the external to the internal structural side [42, 43] (Fig. 12.2).

The Austroalpine is the uppermost super unit, widely exposed in the Eastern Alps. This composite nappe system originated from the ocean-facing (distal) part of the Adriatic passive continental margin, which principally developed in the Cretaceous (Eoalpine) orogeny. The Sesia–Lanzo Zone (eclogitic schists and gneiss) and the Dent Blanche nappe (schists, gabbro, Mesozoic cover, and metagranites) are present in this system.

The Piedmont Zone is characterized by a part of terrigenous flysch-type metasediments (quartzites, calcareous schists and marbles) and one of the prevalent



MAP KEYS

**SOUTH-ALPINE ZONE**

Ivrea Verbano Zone (IV); Canavese Zone (CA)

Canavese Lineament

**AUSTRALPINE ZONE**

in granulitic facies:  
Sesia-Lanzo Zone: 2 Dioritic kinzigitic Zone  
Dent Blanche s.l. nappe

in greenschist facies:  
Sesia-Lanzo Zone: Gneiss Minuti Complex (GM)  
Dent Blanche s.l. nappe: Arolla Unit (AR) M.Mary (MM) Pillonet (P)

in eclogitic facies:  
Sesia-Lanzo Zone: Eclogitic Micaschists Complex (ME)  
Dent Blanche s.l. nappe: Emilius (E) Glacier Refray (GR)

**PIEDMONT ZONE**

Prevailing ocean cover metasediments sector (calc-schist, marble, quartzite)

Prevailing metabasite sector, deriving from oceanic basement (serpentine, amphibolite, metagabbro, prasinite)

**PENNIDIC ZONE**

**Upper Pennidic Zone**  
Monte Rosa (MR) and Gran Paradiso (GP) massifs Arcesa-Brusson (AB)

**Middle Pennidic Zone (G.S Bernardo Nappe)**  
Axial Permo-Carbonifer Zone (Houliere Zone) and outer Briançonnais cover sheets

Ruitor polymetamorphic basement, inner Briançonnais basement and metasedimentary cover sheets. a. Grand Nomenon granodiorite pluton

**Outer Pennidic zone**  
Tarentaise breccia and Scaglie Basali Zone Versoyen Zone; Piccolo S. Bernardo Zone

**Pennidic Frontal Thrust (FP)**

**ULTRAHELVETIC ZONE**

Ultrahelvetic decollement nappe  
M. Chetif and M. Frety nappes

**HELVETIC ZONE**

Monte Bianco massif (paraschist, migmatite, granite) and subordinate mesozoic sedimentary cover units

Fig. 12.2 Geological map of the Aosta Valley [42]. The yellow circle marks the case study location

metabasites derived from the oceanic substrate (leucocratic gneisses, prasinites, metagabbros and serpentinites).

The Pennidic zone has an Upper Pennidic Zone (metaconglomerates, schists, metagranites and gneiss), a Middle Pennidic Zone (dolomites quartzites, gneiss,

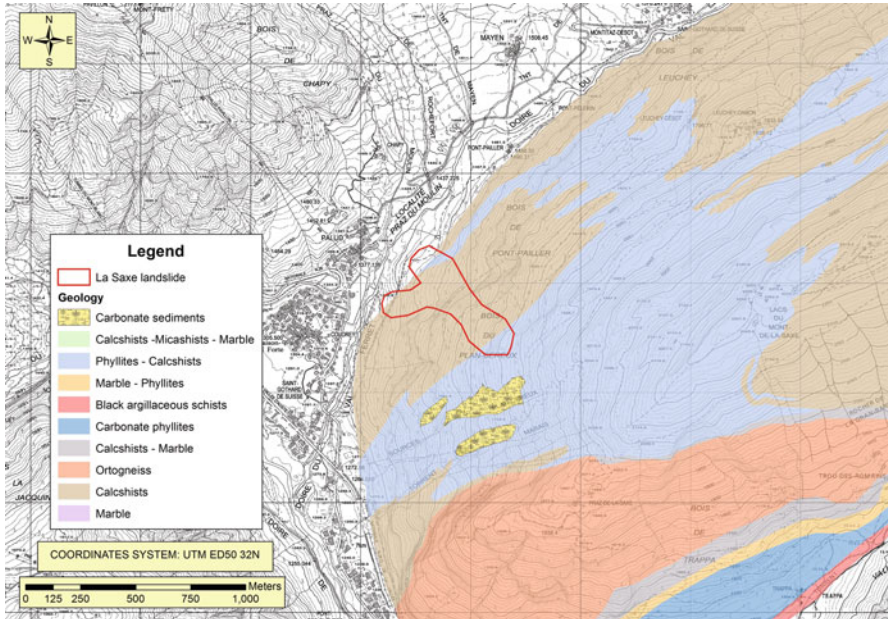


**Fig. 12.3** Geological map of the Mont de La Saxe landslide. The red polygon mark the landslide area

calcareous schists, metagranites and gypsum) and an Outer Penninic Zone (quartzites, prasinites, flysch, serpentinites, calcareous schists and schists).

Our case study, the Mont de la Saxe landslide is situated in the Ultrahelvetic Zone, consisting of, the Mont Chetif nappes (carniole, limestones, calcareous schists, and porfiroids), the Ultraelvetic nappes and the Mont Frety nappes (Fig. 12.3). The Helvetic Zone consists of the Mont Blanc Massif (Granites, migmatites and paraschists) and, subordinately, by the Mesozoic covers sheets (Regione Valle d'Aosta and Università degli Studi di Torino, 2005). Specifically, Mont de la Saxe is situated to the south of the Mont Blanc crystalline Massif, in the western Italian Alps, which originated in the Cretaceous period through the subduction of a Mesozoic ocean and collision between the European and Adriatic continental margins [44]. The study area is located in deformed Middle Jurassic meta-sedimentary sequences, consisting mainly of tightly foliated carbonate-bearing argillaceous schists, black schists and arenaceous limestones with quartz arenites levels [45, 46]. South of the study landslide area, penninic units are found, which comprise the low-grade meta-sedimentary deposits of Courmayeur zone [44]. This unit, dominated by black argillaceous schists, dips towards SE, with angles from 20 to 60°, forming an imbricated structure. The landslide (of about  $8 \times 10^6 \text{ m}^3$ ) extends from 1400 to 1870 m a.s.l., covering an area of approximately 150,000  $\text{m}^2$ . Its maximum horizontal length is around 550 m, maximum width about 420 m, and mean slope gradient 37°. The upper scarp, approximately 200 m wide, is characterized by a steep rock wall some tens of meters high, along subvertical schistosity planes [47] (Fig. 12.3).

## 12.3 Materials and Methods

The landslide analysis is based on multi-temporal higher-resolute datasets collected with a long-range terrestrial laser scanner (TLS) which uses LiDAR technology. The principle is based on the time-of-flight distance measurements using an infrared sensor (near-infrared laser with a wavelength of 1550 nm, a measurement range of 4000 m, an accuracy of 15 mm, a precision of 10 mm) [48].

The general workflow of the study, from the data acquisition to the final elaboration is illustrated in the following.

### 12.3.1 Data Acquisition

During 3 years (from April 2012 to April 2014) a TLS survey (once per year) was executed with the aim of detecting the geomorphological variations (elevation and volume) that characterize the landslide phenomena of the Mont de La Saxe.

Specifically, the TLS was used to acquire and generate a high-resolute 3D point cloud of the investigated area. The scans have been designed to obtain a final ground resolution of 10 cm, which was deemed suitable to capture both large-scale structure and micro-topography [49]. To effectively scan the majority of the landslide zone, scanning has been performed from an elevation higher than the area of interest in order to obtain an oblique point of view from above the landslide. This approach also allows the laser pulse to penetrate deeply in the topographic depression [50, 51]. For this reason, the scan position chosen is located near the Rifugio Pavillon, on the Mont Blanc Massif, at an altitude of 2020 m a.s.l. From this position, a complete survey can be undertaken of the Mont de La Saxe landslide with a long-range laser scanner.

### 12.3.2 Data Elaboration

The first processing step of the 3D point cloud data involves the removal of the isolated points and additional noises data (such as aerosols and water droplets) which may lie around the scan position. Furthermore, a coarse error removal elaboration was implemented on the point cloud. After this procedure, it is necessary to apply an ICP (Iterative Closest Point) algorithm, which is an efficient algorithm for robust rigid registration of 3D data [52] to align multiple scans. The implementations of the ICP allow reducing the standard deviation of the point clouds alignment. In this way, it is possible to merge point cloud from different scan position using an overlap between the scans. The algorithm works at best with planar surfaces in RiSCAN PRO, in this study area we obtained an average 3D error of about 0.02 m.

The third step aims to separate the ground points from the non-ground-point (vegetation). Therefore, a terrain filter tool, compatible with RiSCAN PRO, was used. This filter works in a hierarchic manner with several levels of details, which is based on a grid representation of the data at each level [53]. Since the method may lead to misclassification of a steep area and edges as vegetation, manual checking and correction were performed at the end of the process.

The fourth step uses the registration tool of RiSCAN PRO that allows associating a proper coordinate system to the point cloud using tie point targets (reflectors). Specifically, for the first survey (April 2012), the recording of the coordinates of individual reflectors was undertaken by using a global navigation satellite system (GNSS) receiver. The GNSS data were refined by a post-processing differential correction based on close to the permanent station (Aosta area, 20 km away). One of the scan should at least contain three reflector targets for carrying out the registration by tie points with common point configuration algorithm in RiSCAN PRO software. The other two TLS surveys (April 2013 and April 2014) were aligned using the ICP algorithm based on the first georeferenced survey (April 2012).

Finally, the last step consists of the generation of three DTMs using ArcGIS 10.2 software. The quality of the DTM largely depends on the accuracy of individual survey points and the method of interpolation [54]. Various factors can produce errors in the digital elevation model (DEM), such as topographic complexity, survey point quality, surface composition, sampling strategy and interpolation methods [55–58]. The quality of the raw survey data is of vital importance.

We evaluated the optimal pixel size resolution using the Nyquist-Shannon sampling theorem [59] and generating a density map on LAS-dataset (LAS file is an industry-standard binary format for storing LIDAR data) to analyze the point cloud distribution before evaluating the better resolution to DTM.

According to Lichti et al. 2006, in order to avoid blurring effects (the resolution can be much lower than expected if the beamwidth is larger than the sampling interval), the final DTMs were generated with a resolution of 0.25 m. This operation was carried out by a Natural Neighbor interpolator tool with minimum cell assignment in ArcGIS (10.2) [8, 60]. Natural Neighbor interpolator was chosen as it can leave a coarser morphology avoiding smoothing effects [61].

## 12.4 Results and Discussion

In order to the estimate elevation change and change of volume during 3 years (2012–2014), the elevation difference maps and the erosion and deposition maps were created with TLS-derived DTMs in ArcMap, as shown in Figs. 12.4, 12.5, and 12.6.

Table 12.1 summarizes the change of volume, the volume balance between the erosion and deposition phenomena in the different time intervals.

From 2012 to 2013 (Fig. 12.4), the change of surface elevation was mainly in the middle and up side of the landslide body. Figure 12.5 shows how the change of surface elevation was mainly in the middle and bottom side of the Mont de La Saxe.



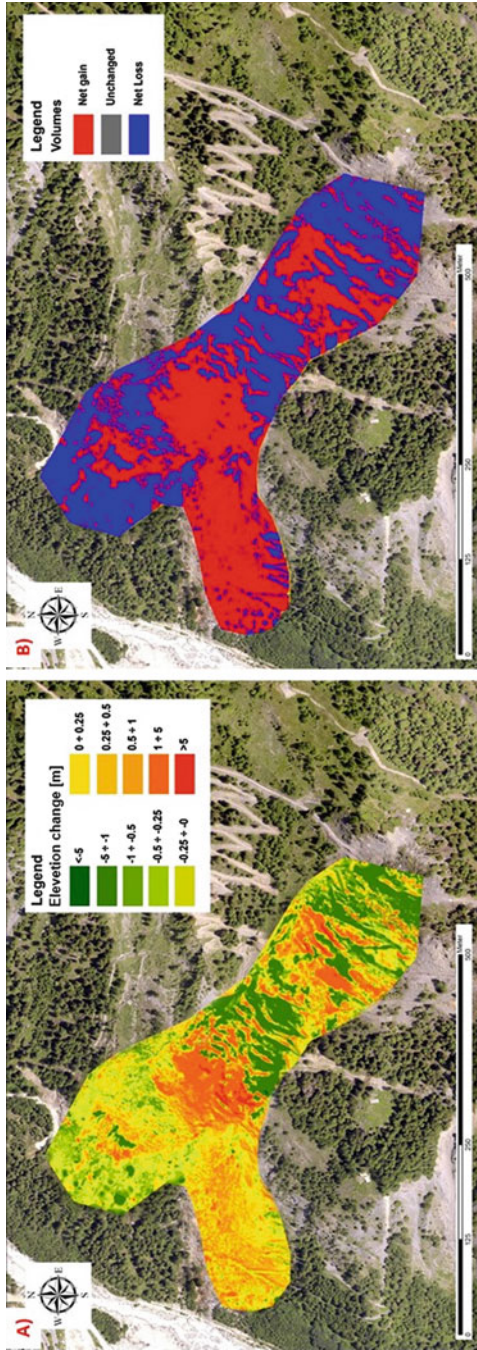


**Fig. 12.4** Elevation and volume change maps of the landslide generated from the comparison between DTMs (2012–2013). (a) Map of elevation change; (b) Map of volume change

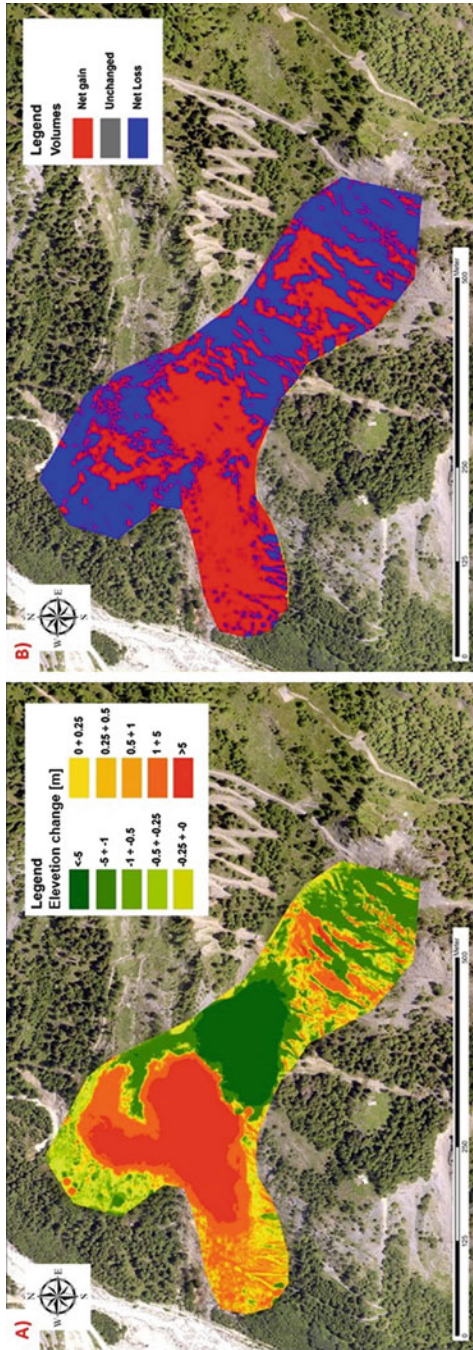


**Fig. 12.5** Elevation and volume change maps of the landslide generated from the comparison between DTMs (2013–2014). (a) Map of elevation change; (b) Map of volume change

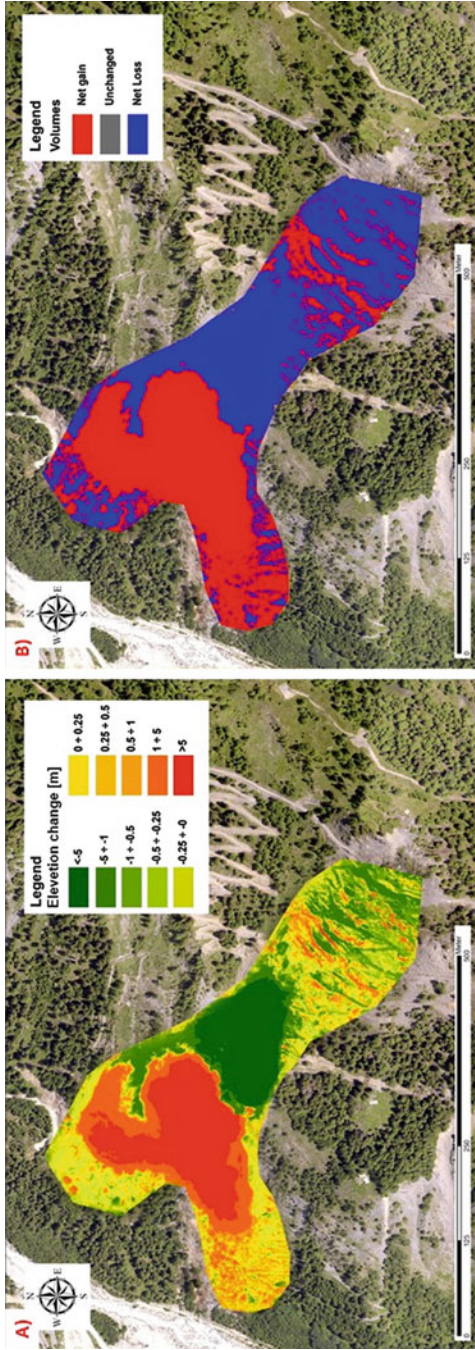


**Fig. 12.6** Elevation and volume change maps of the landslide generated from the comparison between DTMs (2012–2014). (a) Map of elevation change; (b) Map of volume change

Figure 12.6 illustrates the evolution of the landslide between 2012 and 2014, from which it was noticed that the major elevation change occurred in the middle and bottom side of landslide body.

The local uplift reached up to 5 m from 2013 to April 2014, the large erosion happened in the middle zone and the mass movement increased the elevation of the bottom part of the landslide up to 5 m. The acquisitions elaborated from 2012 to 2014, well presents the evolution process of the mass movement phenomena occurred in 2 years. During this period the elevation of the topographic surface in the southwest crown zone decreased significantly. The change primarily consisted in a lowering of the topographic surface in the lower part of the crown zone. The mass flow separated in two directions in the toe zone. The surface elevation in the south part of the landslide toe abruptly changed, producing a deposit with local elevation increased to 10 m. The volume change computed for different time intervals are shown in Table 12.1. These data indicated that the period of 2013–2014 has major changes in volume than the previous year.

During the period 2009–2012 [62] several geophysical surveys were performed on the Mont de La Saxe landslide. Specifically, five seismic tomography profiles were acquired along the landslide slope in 2010 (Fig. 12.7).

**Table 12.1** Change in volume computed for different time intervals based on DTMs

Time interval	Erosion (m <sup>3</sup> )	Deposition (m <sup>3</sup> )	Volume balance (m <sup>3</sup> )
2012–2013	44,238	41,341	2897
2013–2014	246,318	240,602	5716
2012–2014	271,586	261,845	9741

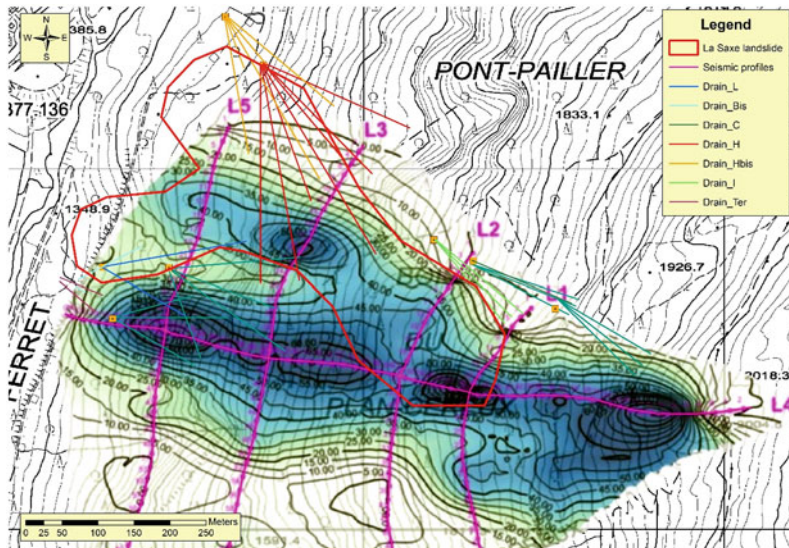


**Fig. 12.7** Seismic profiles map and drain networks in the landslide area

These surveys show that either relaxed or fractured rock masses reaching depths up to 70–90 m are present (blue area in Fig. 12.7). Under these rocks, some relatively sound or slightly relaxed rock was detected. This thickened material tends to decrease in outer direction respect to the geophysical area; however, it maintains an important thickness in the landslide area (40–50 m of depth). Specifically, the areas where the highest values are detected corresponding to the landslide part where the major elevation change occurred on the landslide body.

Moreover, from 2010, several underground water drainage works were installed to reduce the groundwater pressure behind the landslide body (Fig. 12.7). The monitoring of discharge yielded from drainpipes shows that the ones located in NW part of the geophysics area return major values respect to the drainage work located in SW part of that area. So, we can hypothesize that the NW part of the geophysical area is highly influenced by the groundwater flow which affects the stability of the thickened material. This hypothesize seems to be confirmed by the elevation change and the volume variation that identify a major displacement in the middle and the bottom side of landslide body during 2012–2014.

## 12.5 Conclusions

Large landslides can produce significant hazard emergency, so that understanding their mechanism and quantifying precisely the volume displacements require acquisition of accurate datasets. The Mont de La Saxe case study was analyzed through the use of a long-range terrestrial laser scanner (TLS). This instrumentation allowed collecting several point-cloud datasets of the topographic surface of the landslide during 3 years (from 2012 to 2014). These provide a robust multitemporal dataset to study the landslide evolution. The digital surface models, derived from the point clouds, allowed to reconstruct the 3D deformation of the mass movement and to calculate the elevation change and the volumetric changes from 2012 to 2014. The analysis showed how the landslide increased the velocity which consequently increased the displaced volume (66% of the total volume displaced occurred during the 2nd year). The 85% of the total area affected by the landslide underwent a change, showing the size of the phenomena.

Furthermore, monitoring datasets allow the subdivision of the landslide in different zones with different behaviors in terms of elevation and volume changes. The geophysical analysis performed in 2010 showed the presence of thickened material extending to depths up to 40–50 m in the landslide area. Furthermore, drainage work installed in the same period of time indicates that the discharge collected in NW part of the area return major values with respect to the drainage works located in the SW part of that area. So, it seems that groundwater flow affects the stability of the thickened material located in NW part of the area causing landslide movements.

This study shows that how the integration between laser scanner datasets and GIS allows performing a multi-temporal analysis with important results that support the landslides risk assessment and helps to improve the environmental management system for hazard emergency. The future investigation aims to integrate highly

precise topographical measurement with hydrological analysis, with the aim of defining the influence of the hydrogeological system on the local movement of the landslide body.

**Acknowledgments** We thank the Regione Autonoma Valle d’Aosta, Assessorato Opere pubbliche e difesa del suolo – Dipartimento difesa del suolo e risorse idriche for support and data sharing. We are grateful to the anonymous reviewers and Editors for their precious suggestions.

## References

1. Guzzetti F, Reichenbach P, Cardinali M et al (2005) Probabilistic landslide hazard assessment at the basin scale. *Geomorphology* 72(1):272–299
2. Geertsema M, Highland L, Vaugeouis L (2009) Environmental impact of landslides. In: *Landslides—disaster risk reduction*. Springer, Berlin, pp 589–607. doi:[https://doi.org/10.1007/978-3-540-69970-5\\_31](https://doi.org/10.1007/978-3-540-69970-5_31)
3. Refice A, Capolongo D (2002) Probabilistic modeling of uncertainties in earthquake-induced landslide hazard assessment. *Comput Geosci* 28(6):735–749
4. Liu JG, Mason PJ, Clerici N et al (2004) Landslide hazard assessment in the Three Gorges area of the Yangtze river using ASTER imagery: Zigui–Badong. *Geomorphology* 61(1):171–187
5. Pourghasemi HR, Moradi HR, Aghda SF et al (2014) GIS-based landslide susceptibility mapping with probabilistic likelihood ratio and spatial multi-criteria evaluation models (North of Tehran, Iran). *Arab J Geosci* 7(5):1857–1878
6. Nichol JE, Shaker A, Wong MS (2006) Application of high-resolution stereo satellite images to detailed landslide hazard assessment. *Geomorphology* 76(1):68–75
7. Hong Y, Adler R, Huffman G (2006) Evaluation of the potential of NASA multi-satellite precipitation analysis in global landslide hazard assessment. *Geophys Res Lett* 33(22):1–5
8. Prokop A, Panholzer H (2009) Assessing the capability of terrestrial laser scanning for monitoring slow moving landslides. *Nat Hazards Earth Syst Sci* 9(6):1921–1928
9. Abellán A, Calvet J, Vilaplana JM et al (2010) Detection and spatial prediction of rockfalls by means of terrestrial laser scanner monitoring. *Geomorphology* 119(3):162–171
10. Niethammer U, James MR, Rothmund S et al (2012) UAV-based remote sensing of the Super-Sauze landslide: evaluation and results. *Eng Geol* 128:2–11
11. Jebur MN, Pradhan B, Tehrany MS (2014) Optimization of landslide conditioning factors using very high-resolution airborne laser scanning (LiDAR) data at catchment scale. *Remote Sens Environ* 152:150–165
12. Catani F, Casagli N, Ermini L et al (2005) Landslide hazard and risk mapping at catchment scale in the Arno River basin. *Landslides* 2(4):329–342
13. *Landslides in Italy – Special Report 2008* (2008) ISPRA (Italian National Institute for Environmental Protection and Research). Rapporti 83/2008, p 38. ISBN 978-88-448-0355-1
14. Forno MG, Gattiglio M, Gianotti F (2012) Geological context of the Becca France historical landslide (Aosta Valley, NW Italy). *Alpine Medit Quat* 25(2):125–140
15. Barla G, Antolini F, Barla M et al (2010) Monitoring of the Beauregard landslide (Aosta Valley, Italy) using advanced and conventional techniques. *Eng Geol* 116:218–235
16. Luino F (2005) Sequence of instability processes triggered by heavy rainfall in the northern Italy. *Geomorphology* 66:13–39
17. Ghosh A, Tiwari AK, Das S (2015) A GIS based DRASTIC model for assessing groundwater vulnerability of Katri Watershed, Dhanbad, India. *Model Earth Syst Environ* 1(3):1–14
18. Tiwari AK, Singh PK, De Maio M (2016) Evaluation of aquifer vulnerability in a coal mining of India by using GIS-based DRASTIC model. *Arab J Geosci* 9(6):1–15
19. Tiwari AK, Singh AK, Mahato MK (2017) GIS based evaluation of fluoride contamination and assessment of fluoride exposure dose in groundwater of a district in Uttar Pradesh, India. *Hum Ecol Risk Assess* 23(1):56–66

20. Guzzetti F, Carrara A, Cardinali M et al (1999) Landslide hazard evaluation: a review of current techniques and their application in a multi-scale study, Central Italy. *Geomorphology* 31 (1):181–216
21. Singh PK, Tiwari AK, Panigarhy BP, Mahato MK (2013) Water quality indices used for water resources vulnerability assessment using GIS technique: a review. *Int J Earth Sci Eng* 6 (6–1):1594–1160
22. Gupta RP, Joshi BC (1990) Landslide hazard zoning using the GIS approach—a case study from the Ramganga catchment, Himalayas. *Eng Geol* 28(1–2):119–131
23. Aleotti P, Chowdhury R (1999) Landslide hazard assessment: summary review and new perspectives. *Bull Eng Geol Environ* 58(1):21–44
24. Rautela P, Lakhera RC (2000) Landslide risk analysis between Giri and Tons rivers in Himachal Himalaya (India). *Int J Appl Earth Obs Geoinf* 2(3):153–160
25. Temesgen B, Mohammed MU, Korme T (2001) Natural hazard assessment using GIS and remote sensing methods, with particular reference to the landslides in the Wondogenet area, Ethiopia. *Phys Chem Earth Pt C* 26(9):665–675
26. Dai FC, Lee CF (2002) Landslide characteristics and slope instability modeling using GIS, Lantau Island, Hong Kong. *Geomorphology* 42(3):213–228
27. Ayalew L, Yamagishi H (2005) The application of GIS-based logistic regression for landslide susceptibility mapping in the Kakuda-Yahiko Mountains, Central Japan. *Geomorphology* 65 (1):15–31
28. Yalcin A (2008) GIS-based landslide susceptibility mapping using analytical hierarchy process and bivariate statistics in Ardesen (Turkey): comparisons of results and confirmations. *Catena* 72(1):1–12
29. Yilmaz C, Topal T, Süzen ML (2012) GIS-based landslide susceptibility mapping using bivariate statistical analysis in Devrek (Zonguldak-Turkey). *Environ Earth Sci* 65 (7):2161–2178
30. Akgun A, Kincal C, Pradhan B (2012) Application of remote sensing data and GIS for landslide risk assessment as an environmental threat to Izmir city (west Turkey). *Environ Monit Assess* 184(9):5453–5470
31. Perotto-Baldivezo HL, Thurow TL et al (2004) GIS-based spatial analysis and modeling for landslide hazard assessment in steeplands, southern Honduras. *Agric Ecosyst Environ* 103 (1):165–176
32. Tesa G, Galgaro N, Zaltron N et al (2007) Terrestrial laser scanner to detect landslide displacement fields: a new approach. *Int J Remote Sens* 28:3425–3446
33. Bitelli G, Dubbini M, Zanutta A (2004) Terrestrial laser scanning and digital photogrammetry techniques to monitor landslide bodies. *Int Arch Photogramm Remote Sens Spat Infor Sci* 35 (B5):246–251
34. Corsini A, Castagnetti C, Bertacchini E et al (2013) Integrating airborne and multi-temporal long-range terrestrial laser scanning with total station measurements for mapping and monitoring a compound slow moving rock slide. *Earth Surf Process Landforms* 38(11):1330–1338
35. Crosta G, Cancelli P, Tamburini A et al (2012) Chasing a complete understanding of a rapid moving rock-slide: the La Saxe landslide. *EGU General Assembly 2012*. Vienna, Austria
36. Roncella R, Forlani G, Fornari M et al (2014) Landslide monitoring by fixed-base terrestrial stereo-photogrammetry. *ISPRS Ann Photogramm Remote Sens Spat Inf Sci* II-5:297–304. <https://doi.org/10.5194/isprsannals-II-5-297-2014>
37. McKeena J, Roering J (2004) Objective landslide detection and surface morphology mapping using high-resolution airborne laser altimetry. *Geomorphology* 57:331–351
38. Joyce KE, Samsonov S, Manville V, Jongens R et al (2009) Remote sensing data types and techniques for lahar path detection: a case study at Mt Ruapehu, New Zealand. *Remote Sens Environ* 113:1778–1786
39. Kasai M, Ikeda M, Asahina T et al (2009) LiDAR-derived DEM evaluation of deep-seated landslides in a steep and rocky region of Japan. *Geomorphology* 113:57–69

40. Ventura G, Vilardo G, Terranova C et al (2011) Tracking and evolution of complex active landslides by multi-temporal airborne LiDAR data: the Montaguto landslide (Southern Italy). *Remote Sens Environ* 115:3237–3248
41. Mercalli L, Cat Berro D, Montuschi S (2003) Atlante climatico della Valle d'Aosta. Società Meteorologica Subalpina Torino, p 405
42. Bonetto F, Gianotti F (1998) Il Giardino delle Rocce di Pollein. Comune di Pollein, pieghevole
43. Lo Russo S, Amanzio G, Ghione R et al (2015) Recession hydrographs and time series analysis of springs monitoring data: application on porous and shallow aquifers in mountain areas (Aosta Valley). *Environ Earth Sci* 73(11):7415–7434
44. Dal Piaz GV, Bistacchi A, Massironi M (2003) Geological outline of the Alps. *Episodes* 26:175–180
45. Perello P, Piana F, Martinotti G (1999) Nealpine structural features at the boundary between the Penninic and Helvetic domains. *Eclogae Geol Helv* 92:347–359
46. Hölbling D, Füreder P, Antolini A et al (2012) A semi-automated object-based approach for landslide detection validated by persistent scatterer interferometry measures and landslide inventories. *Remote Sens* 4:1310–1336
47. Crosta GB, Prisco C, Frattini P et al (2014) Chasing a complete understanding of the triggering mechanisms of a large rapidly evolving rockslide. *Landslides* 11:747–764
48. Crepaldi S, Zhao Y, Lavy M et al (2015) Landslide analysis by multitemporal terrestrial laser scanning (TLS) data: the Mont de la Saxe landslide. *Rend Online Soc Geol It* 35:92–95
49. Dunning SA, Massey CI, Rosser NJ (2009) Structural and geomorphological features of landslides in the Bhutan Himalaya derived from terrestrial laser scanning. *Geomorphology* 103(1):17–29
50. Schürch P, Densmore AL, Rosser NJ et al (2011) Dynamic controls on erosion and deposition on debris-flow fans. *Geo Soc America* 39(9):827–830
51. Blasone G, Cavalli M, Marchi L et al (2014) Monitoring sediment sources areas in a debris-flow catchment using terrestrial laser scanning. *Catena* 123:23–36
52. Almhdie A, Léger C, Deriche M et al (2007) 3D registration using a new implementation of the ICP algorithm based on a comprehensive lookup matrix: application to medical imaging. *Pattern Recog Letters* 28(12):1523–1533
53. Riegl (2013) RiSCAN PRO operating & processing software for RIEGL 3D laser scanners
54. Heritage GL, Milan DJ, Large ARG et al (2009) Influence of survey strategy and interpolation model on DEM quality. *Geomorphology* 112(3–4):334–344
55. Lane SN (1998) The use of digital terrain modelling in the understanding of dynamic river channel systems. In: Lane SN, Richards K, Chandler J (eds) *Landform monitoring, modelling and analysis*. Wiley, Chichester, pp 311–342
56. Wise SM (1998) The effect of GIS interpolation errors on the use of digital elevation models in geomorphology. In: Lane SN, Richards K, Chandler J (eds) *Landform monitoring, modelling and analysis*. Wiley, Chichester, pp 139–164
57. Wechsler S, Kroll C (2006) Quantifying DEM uncertainty and its effects on topographic parameters. *Photogramm Eng Remote Sens* 72:108–1090
58. Krzysztof S (2009) Evaluation of digital terrain models generated from laser scanning data under forest conditions. MSc thesis submitted in the framework of and according to the requirements of the UNIGIS Master of Science programme (Geographical Information Science & Systems). Jagiellonian University, Kraków, Paris Lodron University of Salzburg
59. Shannon CE (1949) Communication in the presence of noise. *Proc Inst Radio Eng* 37:10–21
60. Bater CW, Coops NC (2009) Evaluating error associated with lidar-derived DEM interpolation. *Comput Geosci* 35(2):289–300
61. Tarolli P, Sofia G, Dalla Fontana G (2012) Geomorphic features extraction from high resolution topography: landslide crowns and bank erosion. *Nat Hazards* 61:65–83
62. Progeo Srl (2010) Indagini geognostiche e geofisiche al di caratterizzare la natura geologico-tecnica del versante in frana in località Coudrey, Courmayeur (AO), frana del Mont de la Saxe